EUROfusion

EUROFUSION CP(15)04/25

G.F. Matthews et al.

Melt Damage to the JET ITER-Like Wall and Divertor

(18th May 2015 – 22nd May 2015)
Aix-en-Provence, France

This work has been carried out within the framework of the EUROfusion Consortium and has received funding from the Euratom research and training programme 2014-2018 under grant agreement No 633053. The views and opinions expressed herein do not necessarily reflect those of the European Commission.

Melt damage to the JET ITER-like Wall and divertor

G.F.Matthews[a*], B.Bazylev[b], A.Baron-Wiechec[a], J.Coenen[c], K.Heinola[d], V.Kiptily[a], H.Maier[e], C.Reux[f], V.Riccardo[a], F.Rimini[a], G.Sergienko[c], V.Thompson[a], A.Widdowson[a]
and JET Contributors[g]

EUROfusion Consortium, JET, Culham Science Centre, Abingdon, OX14 3DB, UK
[a]CCFE, Culham Science Centre, Abingdon, OX14 3DB, UK
[b] Karlsruhe Institute of Technology, INR, P.O.Box 3640, D-76021 Karlsruhe, Germany
[c]Forschungszentrum Jülich GmbH, Institut für Energie- und Klimaforschung – Plasmaphysik, 52425 Jülich, Germany
[d]University of Helsinki, P.O. Box 64, 00560 Helsinki, Finland
[e]Max-Planck-Institut f¨ur Plasmaphysik, Boltzmannstrasse 2, D-85748 Garching, Germany
[f]CEA, IRFM, F-13108 Saint-Paul-lez-Durance, France
[g]Appendix of F. Romanelli et al., Proc. of the 25th IAEA FEC 2014, Saint Petersburg, Russia

**Corresponding author: tel.: 0044 1235 464523, gfm@ccfe.ac.uk (G.F.Matthews)*

Abstract. In October 2014, JET completed a scoping study involving high power scenario development in preparation for DT along with other experiments critical for ITER. These experiments have involved intentional and unintentional melt damage both to bulk beryllium main chamber tiles and to divertor tiles. This paper provides an overview of the findings of concern for machine protection in JET and ITER, illustrating each case with high resolution images taken by remote handling or after removal from the machine. The bulk beryllium upper dump plate tiles and some other protection tiles have been repeatedly flash melted by what we believe to be mainly fast unmitigated disruptions. The flash melting produced in this way is seen at all toroidal locations and the melt layer is driven by $\boldsymbol{j}\times\boldsymbol{B}$ forces radially outward and upwards against gravity. In contrast, the melt pools caused while attempting to use MGI to mitigate deliberately generated runaway electron beams are localised to several limiters and the ejected material appears less influenced by $\boldsymbol{j}\times\boldsymbol{B}$ forces and shows signs of boiling. In the divertor, transient melting of bulk tungsten by ELMs was studied in support of the ITER divertor material decision using a specially prepared divertor module containing an exposed edge. Removal of the module from the machine in 2015 has provided improved imaging of the melt and this confirms that the melt layers are driven by ELMs. No other melt damage to the other 9215 bulk tungsten lamellas has yet been observed.

Keywords: JET, ITER-like Wall, melting, melt layer, beryllium, tungsten

PACS: 52.55.Fa, 52.55.Rk

1 Introduction

Beryllium has a high melting pointing (1285°C) compared to other low atomic number metals. However, beryllium poses more risk than carbon where the operational limit in tokamaks is rather soft and defined by the point at which carbon sublimation starts affecting the plasma significantly (2000-3000°C). It is not just that the maximum allowed operational surface temperature must be lower but also that the existence of a liquid phase raises the prospect of major modifications to the surface profile via melt events. Surface melting can then lead to a degradation of future power handling performance. Given that all main chamber plasma facing components (PFCs) have to be actively cooled in ITER and that the main chamber beryllium cladding is planned to be only 5mm thick, it is clear that understanding melt behaviour in a range of off-normal events is crucial.

Tungsten is now the chosen material for the ITER divertor target [MM2014, RP2011] and with its melting point of 3422°C it provides more headroom before melting occurs than beryllium but the existence of liquid phase poses additional risks compared to carbon. The high atomic number of tungsten (Z=74) also means that in contrast to beryllium (Z=4) it can radiate power efficiently via line radiation even at the high temperatures expected in the core of ITER. While plasmas are known to be very tolerant of beryllium impurities, tungsten radiation can cause collapse of the central temperature and disruptions which may also damage PFCs. For this reason, the stability of W melt layers created by ELMs and impact of any emitted droplets on the plasma has been a concern for ITER and the subject of a dedicated experiment in JET.

In this paper, we describe the latest observations of melt events intentional and otherwise seen in experiments with JET's ITER-like Wall [GFM2011]. The results show complex behaviour that may at first seem counter intuitive. Our goal for this paper is to provide a qualitative overview along with current thinking as to the dominant physics involved and an insight into the operational consequences for JET.

2 Main chamber beryllium components

The design objective for the JET ITER-like Wall was to ensure that bulk Be tiles formed the first point of contact between the plasma and the main chamber wall. Tungsten coated CFC and Be coated Inconel tiles are used but only in recessed areas [VR2009]. No intentional Be melting experiments were carried out but melting has none-the-less occurred with the melt behaviour being dependent on the event type.

2.1 Slow melting of Be limiters

The simplest type of Be melt event to imagine is a slow heating up of JET's inertially cooled bulk beryllium limiters to melting point. A series of experiments were carried out on JET in 2012 which were intended to explore the power handling limits of the Be limiter geometry [VT2007] without exceeding them. A calibrated tangential wide angle medium wavelength infra-red camera (KL7) was used to diagnose the limiter temperatures in one JET octant. Despite careful monitoring, melting of the inner Be limiters occurred. A contributory factor to this was the existence of a narrow heat flux feature close to the separatrix in inner wall limiter configurations leading to unexpected toroidal asymmetries in the heat flux [GA2013]. The resulting melt created a jet of molten beryllium which travelled up the surface of the limiter perpendicular to the magnetic field as shown in figure 2.1.1. This behaviour is first described in a paper by Sergienko *et al.*[GS2013].

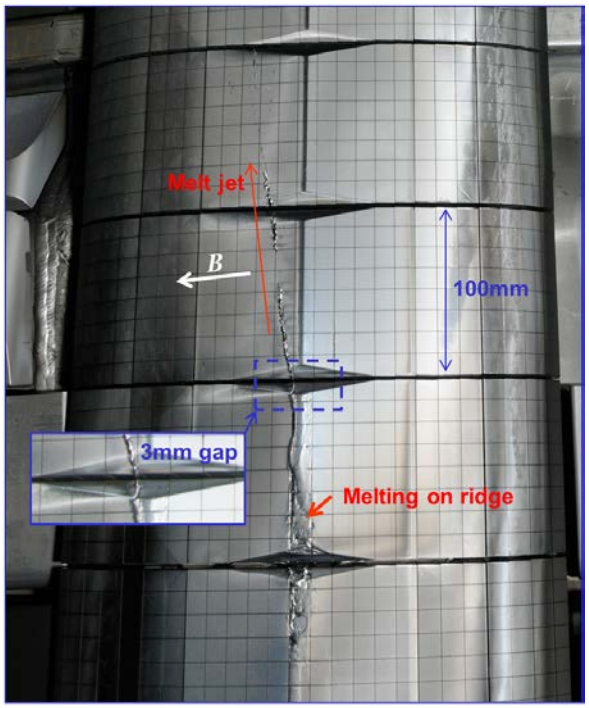

Figure 2.1.1 Bulk beryllium melting on the ridge of the JET inner wall limiter (4X).

Previous experiments on melt layers motion in TEXTOR were focused on tungsten and reported similar gravity defying behaviour [GS2007]. In this case the motion was found consistent with $\boldsymbol{j}\times\boldsymbol{B}$ forces with the dominant component of the current arising from thermal electron emission which is high at the melting point of tungsten. Calculations for the TEXTOR case predicted thermal emission currents up to $1.2\mathrm{MAm}^{-2}$. Beryllium has a much lower melting point and a very much lower thermal electron emission current. Just to overcome gravity the net current density flowing into a liquid surface needs to satisfy $j_{\perp} > \rho g/B$ where B is local magnetic field, ρ is the liquid density and g is the local

acceleration due to gravity [GS2013]. In the case of beryllium this means we need >6kAm^{-2} to explain the upward movement and the thermal electron emission only just reaches this value at the boiling point. The alternative source of the current proposed by Sergienko *et al.*[GS2013] was that due to a net current from the plasma driven by high secondary electron emission. For a plasma with a separatrix plasma density of 10^{18}m^{-3} and electron temperature of 100eV the ion/electron flux to a floating surface is ~8kAm^{-2} and densities several times this are reasonable for the JET cases. However, there has to be a mechanism to retard or cancel the electron current to the surface so that a net positive current of the right magnitude results and the proposed secondary electron emission mechanism is a speculation which cannot be proven with the available data from JET.

Another feature pointed out by Sergienko *et al.*[GS2013] is the apparent ability of the liquid Be jet to leave the surface and re-attach itself further on. The inner wall guard limiters curve in at the top and melt zone was above the mid-plane so gravity is always trying to pull the liquid down and away from the surface. At the same time, current flow into the surface is driving the liquid upward along the limiter surface as shown in figure 2.1.2(a). If gravity wins out and the liquid stream pulls away from the surface as shown in figure 2.1.2(b), the current flow to the surface $j_{\perp}$ is interrupted and replaced by a current flow along the stream $j_{||}$ which will push the jet back onto the surface and if a bridge is formed the shear forces can eject a part of the liquid stream into the plasma, figure 2.1.2(c).

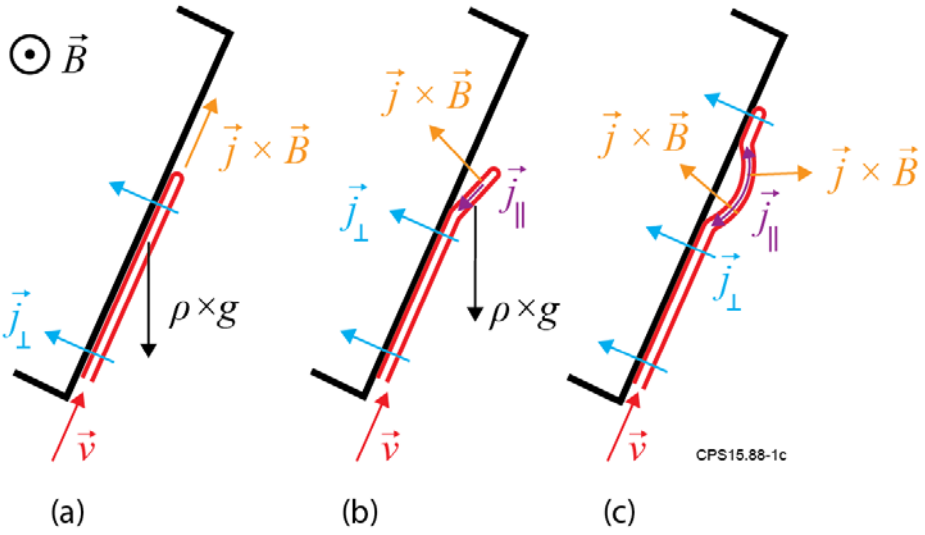

Figure 2.1.2: (a) Schematic showing a current ($j_{\perp}$) arriving from the plasma and passing through a liquid Be layer (red) and into the solid Be limiter surface. (b) If the liquid layer leaves the surface a parallel current $j_{||}$ arises and the resulting ***j***×***B*** *force* pushes back. *(c) If a bridge is produced then the opposing* ***j***×***B*** *forces may shear the layer apart.*

The idea of current flow from the plasma appears to explain rather well the main features we observe. There is one aspect however that seems hard to reconcile and this can be seen in the enlarged section of figure 2.1.1. Between each of the inner wall limiter tile assemblies there is a 3mm gap. The ridges of adjoining tiles have triangular chamfers at the gap which creates a shallow valley which should be shadowed from the plasma near its bottom. The mystery is how the stream of liquid Be is driven across the shadowed zone and how it crosses a 3mm gap before setting off again up the slope on the other side. Build up material in the gap to create a bridge is a possible means for crossing the gap but the images tend not to support this although the ultimate test would be removal of the tiles for examination which has not yet been done.

2.2 Fast melting of Be PFCs by disruptions

Changing the dominant material of JET main wall from all carbon to beryllium had a profound impact on the physics of disruptions [PdeV2012]. The energy radiated during disruptions was up to a factor 5 lower with 50-90% of the available plasma thermal and magnetic energy being dumped on the wall. Although disruptions with JET's ITER-like wall tend to have longer current quench times due to the

higher plasma temperatures, fast vertical displacement events (VDEs) can still occur either accidently or deliberately resulting in current quench times ~10ms. In JET, disrupting plasmas usually move upwards and inwards and interact with the Be upper dump plate tiles as shown in figure 2.2.1.

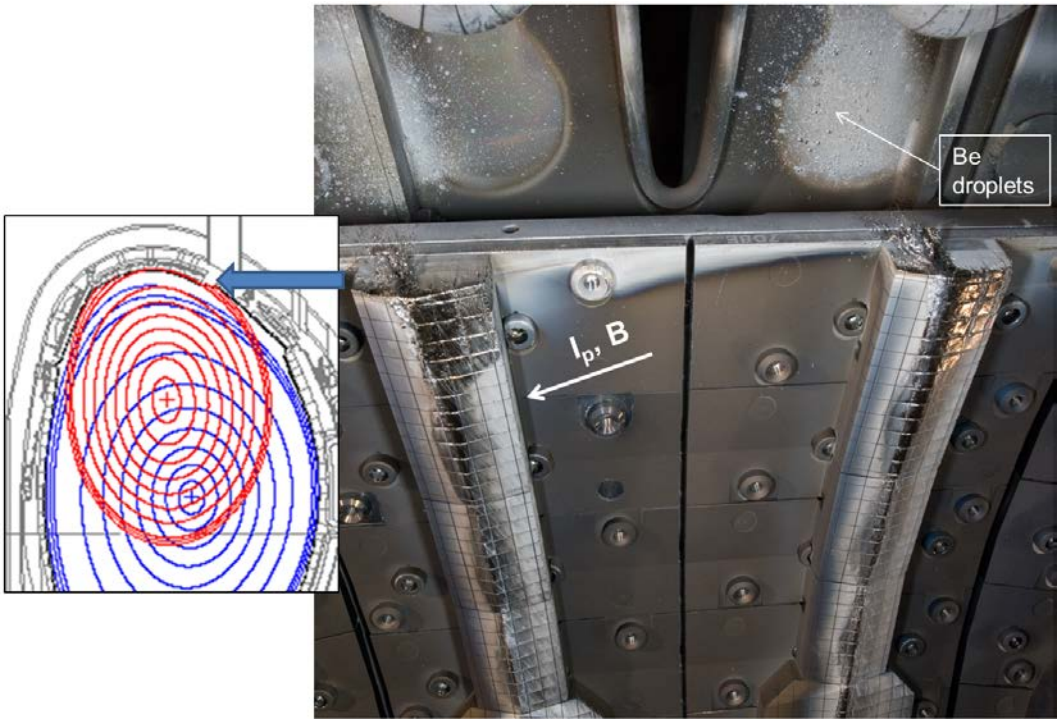

Figure 2.2.1 JET plasmas usually move upwards and inwards during disruptions and can cause melt damage to the beryllium upper dump plate tiles, particularly near the outer ends which are a series of 64 ribs. The stress relieving castellations on the Be tiles are 12mm square.

Dump plate tile melting was observed in early disruption experiments with the new ITER-like Wall and led to restrictions on the allowed plasma current for operation without the system for disruption mitigation by massive gas injection (MGI) enabled [ML2011]. Initially, the limit was set by the plasma current alone until a series of heated plasmas used for testing forces due to VDEs caused much of melting which visible in figure 2.2.1. Now MGI must be used in disruptions where $W_{thermal}$(MJ) > 5-I_p^2(MA) so that the total deliverable thermal and magnetic energy is kept below 5MJ.

As with the bulk melting of the Be limiters described in section 2.1, the disruption driven melt layer motion on the dump plates is dominated by $\boldsymbol{j}\times\boldsymbol{B}$ forces. The melt layers are driven perpendicular to $\boldsymbol{B}$ along the surface of the tiles towards the outboard ends of the dump plate ribs. On reaching the end of the outermost dump-plate tile the melt layer turns through 90° and heads almost vertically up like an inverted water fall. Eventually the liquid Be parts company with the end of the tile and a spray of Be droplets is deposited on Inconel vacuum vessel wall at the top of the machine. As before, the driving force which propels the liquid along the tile surface comes from current flow into the liquid layer, figure 2.1.2(a), but in this case the dominant source of current is most likely to be the halo current which can provide ~100kAm^{-2} per MA of plasma current. This is more than an order of magnitude higher than the gravitational force on the liquid layer. The schematic of figure 2.1.2(b) shows how a parallel current arises in a liquid layer if it leaves the surface which will push it back into electrical contact. The same process can explain how it is possible for the liquid layer to make the sharp right angle turn at the tile end. As the layer moves up the tile end will eventually become shadowed from the halo current. At this point the electromagnetic forces keeping it stuck to the surface and driving it along will disappear and if it has enough forward momentum it will leave the surface in a spray of droplets may stick to Inconel vacuum vessel wall at the top of the machine, figure 2.2.1.

The melting of the upper dump-plate tiles appears toroidally quite uniform although this could be partly the effect of averaging over many disruptions. The pitch of the tile ridge at the end is ~17° and melting occurs along the ridge with a preference for the side with the long connection length. The

melted area extends further down the tile near the tile end due to field line helicity/penetration. The melt layer generated by each disruption is clearly very shallow. This thickness has not yet been directly measured but is clearly << 1mm which is consistent with surface heating and the $t^{0.5}$ scaling of heat diffusion. This can be compared to the bulk melting of section 2.1 which is > 1mm in depth. The energy density at which Be melting occurs from a starting temperature of 200°C is $Q > 20\ t^{0.5}$ (MJ m^{-2} $s^{0.5}$). The current quench in a VDE is ~10ms but the plasma is moving all this time so the true interaction time must be shorter so the energy density must be > 2MJm^{-2}. The empirical energy limit set at JET for use of MGI (5MJ) and this implies an interaction area of 1-2m^2 which is consistent with all 64 dump plate ribs being involved each with tens of cm^2 of shallow melt damage.

Bridging of the 0.35mm wide castellations by the melt layer is widely visible and is also seen in some of the 1.55mm gaps between dump plate tiles. Surface forces may make it hard for molten beryllium to penetrate the narrowest gaps. Also, once inside a gap the layer is out of sight of the plasma so there is no perpendicular current to drive the melt layer further down the side as happens at the exposed tile end. The melt layer may therefore solidify near the top to form a bridge but the relevant tiles were not removed from JET during the current shutdown so this interpretation cannot yet be verified.

2.3 Runaway electron impacts on main chamber PFCs

Since installation of the ITER-like wall, runaway electrons (REs) have not been generated in the aftermath of natural JET disruptions but are considered to a serious risk for ITER PFCs [Papp2013]. With the ITER-like Wall REs need to be produced deliberately using argon MGI to trigger disruptions. In order to test RE mitigation techniques [Reux2015] limiter plasma configurations were used to maximise the natural lifetime of such RE beams to ~100ms Runaway currents of ~1MA were produced in this way and a second MGI injection into the RE plateau using >2000Pa m^3 of Xe or Kr seemed to have no noticeable effect on the RE beam current or energy. As a consequence, there were a number of RE strikes on the Be PFCs in the upper part of the machine leading to significant melting. Figure 2.3.1, shows a typical example of the Be melting that occurred when REs hit the upper section of the inner limiter in pulse #86801. The wide angle infra-red camera saw ejection of molten material from this area when a plasma with a 0.9MA RE plateau was lost to the inner limiter [Reux2015].

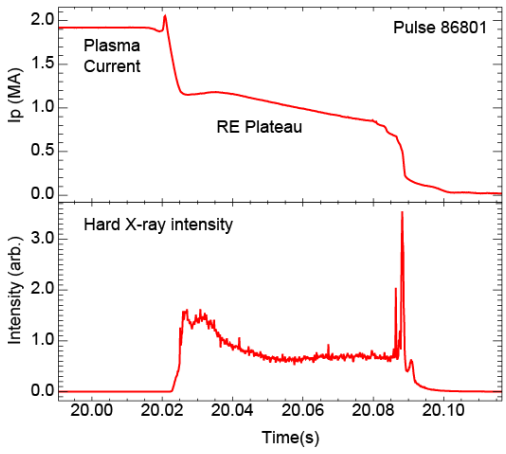

(a)

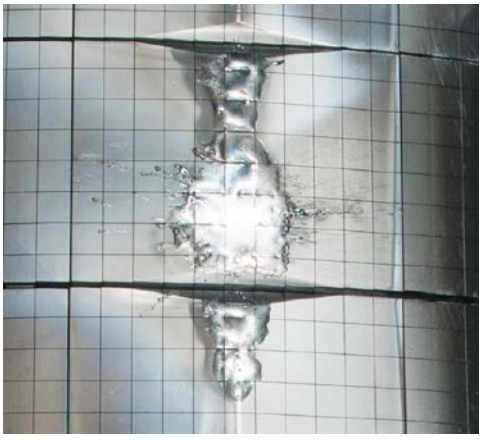

(b)

Figure 2.3.1 (a) Plasma current vs time for JET pulse #86801 in which runaway electron plateau characterised by hard X-ray emission is produced when argon is injected at 20s. (b) In-vessel image of melt damage due runaway electrons from pulse #86801 in which REs hit the tops of the inner wall limiters about 60ms after they are created. The castellations are 12mm square.

An analysis of the gamma spectrum averaged across the RE current plateau using a BGO detector on a horizontal chord suggests a fairly narrow energy distribution for the electrons with average 12.9MeV, figure 2.3.2. The actual energy at the time of impact is not known because the plasma moves out of the field of view but a NaI detector on a vertical chord sees the energy decrease to around 3MeV later in the plateau. This may however be a geometric effect since the RE spatial distribution can be complex.

The RE beams circulate in an anti-clockwise direction arriving on the left hand side of picture 2.3.1 (b). Although the interaction with the limiter occurs on a short timescale we see relatively deep melting compared to that seen due to VDEs and the melt zone is quite symmetric right to left. The reason for this is that the range of runaway electrons in Be at an energy of 12.9MeV is ~4cm which provides a volumetric sources of heating. RE energies up to ~20MeV are observed in JET. Electron ranges in solid beryllium from the continuous slowing down approximation (CSDA) are plotted in figure 2.3.2 using data from the ESTAR code [ESTAR]. Electrons arriving near the apex can therefore pass right through the Be limiter.

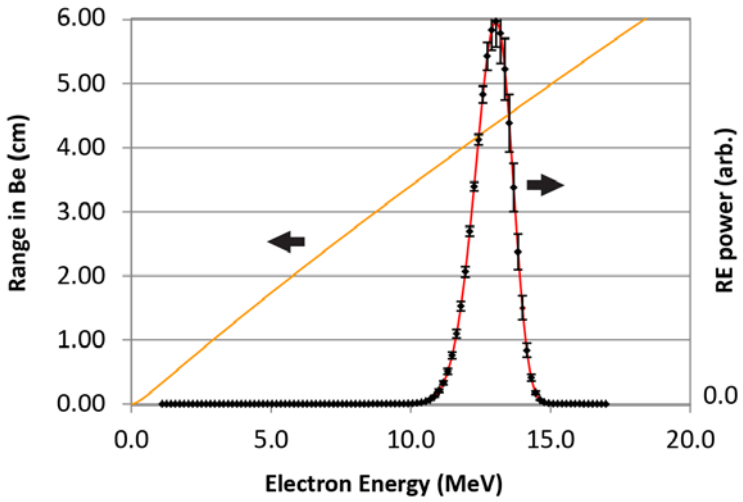

Figure 2.3.2: Range of electrons for solid beryllium as a function of energy from the CSDA range calculated by the ESTAR code [ESTAR] and RE power distribution from fit to gamma spectrum averaged over the current plateau.

Another interesting feature of the melt pattern of 2.3.1(b) is that it is also fairly up/down symmetric despite the fact that the current density from the beam must be easily of sufficient magnitude to drive similar strong $\boldsymbol{J}\times\boldsymbol{B}$ motion to that seen in the slow limiter melting and fast disruption melts described in sections 2.1 and 2.2. The REs which arrive from the left of image 2.3.1(b) can pass through the melted material they create. The current due to the beam itself is aligned with the magnetic field and net perpendicular current can only be generated when the electrons eventually slow down. If sufficient perpendicular electron current were deposited or somehow induced, the melted Be would be pushed down the limiter i.e. the opposite direction to that seen in figure 2.1.1.

In the image 2.3.1(b) we can also see what look like bubbles which were frozen in when the molten Be re-solidified and these features are even clearer elsewhere. This suggests that boiling may have occurred although the physics of boiling under these conditions of low pressure and large transient heat flux are difficult to predict. The heat of vaporisation of beryllium is ~32kJg^{-1} which can be compared with the heat of fusion which is 1.3kJg^{-1} and the energy required to raise a piece of JET Be PFC from 200°C to melting which is ~3kJg^{-1}. The total energy available in MJ from the REs is given by $W_{RE} \sim I_{RE}\, E_{RE}\, 2\pi R/c$ where c is the speed of light (m/s), R is the major radius of runaway beam (m), I_{RE} is the runaway current (MA) and E_{RE} the runaway electron energy (MeV). If all the ~0.5MA of current that is lost in pulse #86801 towards the end of the RE plateau were carried by 12.9MeV electrons, the kinetic energy available would be ~0.3MJ. This could be fully absorbed by vaporising ~5cm^3 of beryllium or melting ~70cm^3 of Be. Heating of larger volumes to less than melting is also possible and so these estimates are illustrative of the upper limits for these processes.

The RE damage in #86801 extends toroidally over several nearby limiters then fades away but the overall pattern is complex as is summarised in [Reux2015]. The complexity probably arises from the MHD instabilities which dump the REs on the PFCs but also from inhomogeneity in the spatial distribution of the REs within the plasma column.

Predictive modelling of RE impacts on the JET Be upper dump plate tiles was carried out using the ENDEP and MEMOS codes at a time when no relevant experimental data was available from JET

[Bazylev2013]. Although the codes include a lot of detailed physics of beam interaction with Be and heat transport which captures many of the issues such as the bulk heating due to the electron range which we have discussed more qualitatively. It also includes surfaces forces which are more difficult to estimate and these are particularly important for shallow melt layers. However, this paper also demonstrates that useful predictions were almost impossible to make mainly due to uncertainties in the parameters of the incident REs. In the scenario considered 10kA of runaways at 5MeV interact with $0.6m^2$ of dump plate and create a 0.5mm deep melt layer. In view of this prediction, the damage actually experienced in JET seems rather modest.

3 Divertor tungsten components

The JET ITER-like Wall tungsten divertor was implemented using tungsten coated carbon fibre composite (CFC) tiles and a single row of bulk tungsten tiles [PhM2011]. There are 48 bulk W tile modules each containing 8 stacks of 24 tungsten lamellas giving a total of 9216 lamellas each ~6mm wide in the toroidal direction. This segmented design has been chosen to minimise the risk of cracking the brittle tungsten elements due to thermal stresses and other forces. No melt damage has yet been observed on the normal tungsten lamellas. This suggests that JET procedures and protection systems are achieving their desired goal [VR2014].

3.1 Transient tungsten melting by ELMs

In 2013 a dedicated experiment was carried out using a specially engineered divertor module with the aim of studying ELM-induced transient melting to help ITER reach a decision on the material for its first divertor. The leading edge of a special lamella was exposed to maximise the transient heat load due to ELMs. Melt motion driven by $\boldsymbol{J}\times\boldsymbol{B}$ forces was observed moving material along the exposed edge into the private region where it re-solidified [Coenen2015]. One limitation of this experiment was that the IR camera did not have sufficient spatial resolution to directly resolve the melt layer temperature. Indirect evidence was used to distinguish W melt layer motion driven by ELMs from the type of slow bulk melting behaviour described in section 2.1 for beryllium. Since this work was published however, the module containing the special lamella has been removed from JET and photographed. Excerpts from these images help clarify some of the issues and are shown in figure 3.1.1.

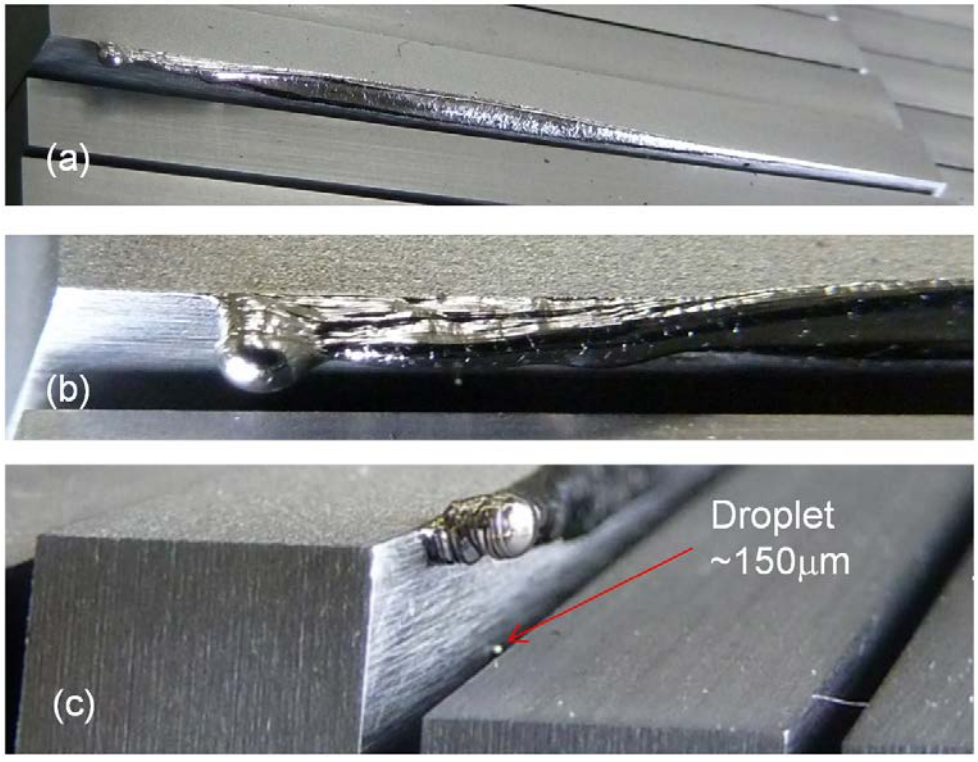

Figure 3.1-1: (a) Image of the melted edge of the special tungsten lamella. (b) Detail of layering of the migrated material. (c) End view showing a droplet adhered to the side of the lamella.

The large layered droplet structure seen in figure 3.1-1(b) first appeared after the third pulse in a series of 7 very similar melt pulses and grew in each subsequent pulse. Although the majority of the material appeared in about 3 pulses, you can count at least 15 discrete layers in the image although there may be many more. The most obvious explanation for this structure is that these are due melt layers which were driven by ELMs.

In figure 3.1-1(a) and (c) we can see that the eroded edge geometry funnels the liquid W into a narrower deeper stream which gives rise to the structure seen in (b). This probably explains why the droplet (b) did not appear in the first two pulses even though erosion of the edge and transport of material along the surface was visible.

During the melt experiment no direct evidence of droplet emission from the lamella was obtained. Data from spectroscopic diagnostics and soft X-rays was however used to conclude that a number of W droplets with diameters of around 100μm had been emitted. Although surface analysis will be needed to confirm its composition, a droplet with a diameter of ~150μm is visible in figure 3.1-1(c) thus supporting the original conclusions.

Simulation of the JET W melt experiment using the MEMOS code [Coenen2015][Bazylev2014] suggests that there is a thermal electron generated current density of up 1000kAm^{-2} during ELMs which drives the layer. This current is at least an order of magnitude larger than the currents available to drive the beryllium motion discussed in sections 2.1 and 2.2. However, due to the fact that the density of tungsten is about 10 times higher than beryllium, ~60kAm^{-2} of perpendicular current are required to compete with gravity. MEMOS simulation of the JET experiment with the thermal electron current switched off show that the surface tension gradient and plasma pressure on their own produce about 5 times less deformation of the surface and a much more symmetrical pattern than is observed [Coenen2015]. There are direct measurements of net current flow to W surfaces in TEXTOR for steady state melting. The data fit the expected temperature dependence of the thermal electron emission model rather well [GS2007, Coenen2011].

4 Conclusions and Outlook

Our purpose here has been to compare and contrast the different types of melt damage and melt motion seen on beryllium and tungsten components in JET. $\boldsymbol{J}\times\boldsymbol{B}$ forces dominate in the balance of forces in every case with the exception of melt pools created by high energy runaway electrons. The source of the current is thought to be different in each case. Slow thermal melts of the Be inner wall limiter may draw ion current from the plasma due to secondary electron emission, Be melt layers produced in fast disruptions may be driven by halo currents and transient W melt layers produced by ELMs are thought to be driven by thermal electron emission.

The next step in understanding the different melt layer behaviours reported here will be laboratory based studies of the morphology of the melt zones and layers. Some of this work is in progress but more tiles will also have to be removed from JET in a future shutdown. Closer examination and cutting will provide further insight into open questions such as how molten beryllium bridges or crosses tile to tile gaps and castellations.

Further progress is also expected from a new W melt experiment using the special lamella shown in figure 4-1. The parallel heat flux will hit the new lamella at an angle of about 17° which is very similar to the Be upper dump plate tiles discussed in section 2.2. The main purpose of the new geometry is fully resolve the surface temperature with the IR camera system to better constrain the melt layer modelling, provide a more ITER relevant geometry and provide insight into the heat flux mitigation factors which were observed in the first experiment [GA2014].

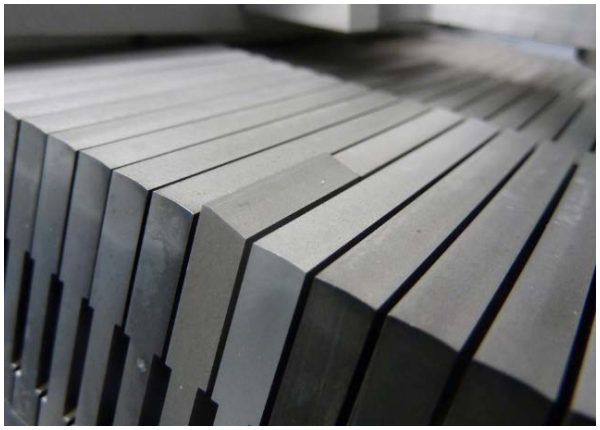

Figure 4-1. New special lamella installed in the JET divertor ready for a new transient W melting experiment in 2015.

5 Acknowledgements

This work has been carried out within the framework of the EUROfusion Consortium and has received funding from the Euratom research and training programme 2014-2018 under grant agreement No 633053. The views and opinions expressed may not reflect those of the European Commission. This work was also part-funded by the RCUK Energy Programme under grant EP/I501045.

6 References

[MM2014] M.Merola *et al.*, Fusion Engineering and Design 89 (2014) 890–895

[RP2011] Pitts R. *et al* 2011 *J. Nucl. Mater.* **415** (Suppl.) S957–64

[VR2009] V. Riccardo et al., Journal of Nuclear Material 390-391 (2009) 895-899

[VR2014] V.Riccardo et al., Fusion Engineering and Design 89 (2014) 1059–1063

[VT2007] V.Thompson, Fusion Engineering and Design 82 (2007) 1706–1712

[GFM2011] G.F.Matthews et al., 2011 Phys. Scr. 2011 014001

[GS2007] G.Sergienko et al., Phys. Scr. **T128** (2007) 81–86

[GS2013] G.Sergienko et al., Phys. Scr. **T159** (2014) 014041 (5pp)

[GA2013] G.Arnoux et al., Nucl. Fusion **53** (2013) 073016 (12pp)

[PdeV2012] P.C. de Vries et al., Plasma Phys. Control. Fusion **54** (2012) 124032 (9pp)

[ML2011] M.Lehnen et al., Nucl. Fusion **51** (2011) 123010 (12pp)

[Papp2013] G.Papp et al., Nucl. Fusion **53** (2013) 123017 (11pp)

[Reux2015] C.Reux et al., Nucl. Fusion in press (2015) “Runaway electron beam generation and mitigation during disruptions at JET-ILW”

[ESTAR] M.J.Berger et al., “Stopping-power and range tables for electrons protons and helium ions”, NISTIR 4999, NIST physical measurements laboratory, http://www.nist.gov/pml/data/star/

[Bazylev2013] B.Bazylev et al., Journal of Nuclear Materials 438 (2013) S237–S240

[Coenen2015] J.W.Coenen et al., Nucl. Fusion **55** (2015) 023010 (22pp)

[PhM2011] Ph. Mertens, Phys. Scr. **T145** (2011) 014002 (7pp)

[Bazylev2014] B.Bazylev et al., Bazylev B. *et al* 2014 PSI 2014 *J. Nucl. Mater.* in press

[Coenen2011] Coenen, J. W.; et al., *Nuclear Fusion, IAEA*, **2011**, *51*, 083008

[GA2014] G.Arnoux et al., Arnoux G. *et al* 2014 PSI 2014 *J. Nucl. Mater.* in press